Published in final edited form as:

*Proc IEEE Conf Decis Control*. 2012 December ; 2012: 1645–1650. doi:10.1109/cdc.2012.6426098.

# A Point Process Model-based Framework Reveals Reinforcement Mechanisms in Striatum during High Frequency STN DBS

**Sabato Santaniello [Member, IEEE]**,
Department of Biomedical Engineering, Johns Hopkins University, Baltimore, MD 21218 USA

**John T. Gale**,
Kent State University, Kent, OH 44242 USA

Department of Neurosciences and the Center for Neurological Restoration, Cleveland Clinic, Cleveland, OH 44195 USA

**Erwin B. Montgomery Jr.**,
Department of Neurology, University of Alabama at Birmingham, Birmingham, AL 35294 USA

**Sridevi V. Sarma [Member, IEEE]**
Department of Biomedical Engineering, Johns Hopkins University, Baltimore, MD 21218 USA

## Abstract

Striatum is a major stage of the motor loop but, despite a pivotal role in the execution of movements, it has been poorly studied thus far under Parkinsonian conditions and Deep Brain Stimulation (DBS). We propose a computational framework to analyze the spiking activity of striatal neurons under several conditions. This framework combines point process models and single unit recordings, and separately evaluates the effects of the spiking history, DBS frequency, and other cells on the neuronal discharge pattern, thus giving a full characterization of non-stationary neuronal dynamics and inter-neuronal dependencies. We applied this framework to 166 striatal neurons collected in a monkey both at rest and during DBS (30–130 Hz). Our analysis was conducted both before and after treatment of the animal with 1-methyl-4-phenyl-1,2,3,6-tetrahydropyridine (MPTP), which evoked Parkinsonian-like motor disorders. We reported that high frequency (≥100 Hz) DBS reduces non-stationary dynamics and inter-neuronal dependencies by regularizing the discharge patterns both in MPTP and normal striatum, while the combination of MPTP and low frequency (30–80 Hz) DBS enhances these features, thus suggesting that pattern regularization in striatum might contribute to the therapeutic effect of high frequency DBS and presumably results from the overlap of feed-forward and feedback activation along the motor loop (reinforcement).

ssantan5@jhu.edu.

## I. INTRODUCTION

High frequency (HF) Deep Brain Stimulation (DBS) of the basal ganglia and thalamus is clinically recognized to treat movement disorders in Parkinson's disease (PD) [1]–[3], but its therapeutic mechanisms still require investigation [4][5]. Most of the studies conducted thus far on single unit recordings, both in humans and animals, have been focused on the local effects of DBS on the stimulation target and the structures downstream (STN, GPi, GPe, thalamus, or cortex, Fig. 1) [6]–[16]. Very little attention has been paid, instead, to the fact that the motor loop is a cycle (Fig. 1) and changes occurring in the structures upstream (e.g., striatum) project downstream to reinforce the local effects of PD and DBS. As an evidence, Montgomery *et al.* [17] recently reported that DBS of the striatum is as effective as DBS of any other structure of the basal ganglia to suppress bradykinesia (one of the main PD symptoms) in humans, thus indicating that the topology of the motor loop plays a pivotal role in the therapeutic mechanisms of DBS.

The striatum is the major stage of the closed-loop in Fig. 1 because of the amount of projections and the wide array of functions performed [18], but, despite of its role, it has been poorly studied thus far. In particular, it is still debated (i) how DBS affects the discharge patterns and pair-wise interactions between striatal neurons (inter-neuronal dependencies), (ii) if the effects of DBS vary with the stimulation frequency, and (iii) how PD impacts the striatal response to DBS.

These questions are important because they may help to understand the role of striatum in the generation of PD-related pathologic rhythms along the motor loop, and the therapeutic mechanisms of HF DBS. We addressed these questions by developing a computational framework that combines point process models and single unit recordings.

In particular, we collected 166 striatal neurons from a monkey that quietly sat in a loosely restraining chair while regular DBS was applied in the STN [19]. The animal was not involved in any motor task to avoid changes in striatal activity related to movement initiation or execution [20]. Multiple DBS frequencies were tested for each neuron (30 to 130 Hz), and the recordings were performed before and after treatment with 1-methyl-4-phenyl-1,2,3,6-tetrahydropyridine (MPTP), which induced severe PD-like motor disorders. For each neuron, disease condition, and stimulation setting, a point process model [21] was computed to capture recurrent non-stationary patterns and inter-neuronal dependencies both before and during DBS.

Point process models have been applied to a wide range of neural systems [22]–[26] and describe the spiking propensity of a neuron as a function of multiple factors (e.g., DBS, ensemble neurons' spiking history, etc.). Point process models were recently used to analyze the discharge pattern of neurons in STN, GPi and motor cortex in PD patients and MPTP-treated monkeys [27]–[29]. Preliminary results of this study were presented in [30].

# II. METHODS

## A. Experimental Setup

A male non-human primate (macaca mulatta) was trained to sit quietly in a loosely restraining chair designed to allow passive movements of the upper and lower limbs while preventing the animal from disturbing the recording instruments. The research protocol was in compliance with “The National Institutes of Health Guide for Care and Use of Laboratory Animals” and approved by the Institutional Animal Care and Use Committee. Details are in [19][31].

Briefly, the animal was implanted with a recording chamber and received STN DBS via a reduced scale model of the human DBS lead (four contacts, each contact being 0.525 mm in diameter, 0.5 mm long, 0.5 mm between contacts, area 0.82 $mm^2$). The electrical stimulation consisted of constant-current symmetric biphasic square-wave pulses, which were delivered between the most distal and the most proximal contact. For each pulse the cathodic phase preceded the anodic phase at the most distal contact (reverse for the most proximal one). Pulse width was 90 μs/phase and amplitude was 80% of the current inducing tonic contraction (0.55 mA), presumably from current spread to the internal capsule. The amplitude producing tonic contraction was determined during 130 Hz DBS. Stimulation frequencies included in this study are: 30, 50, 80, 100, and 130 Hz.

Microelectrode recordings were collected from separate sites of the striatum (caudate nucleus and putamen) on a semi-daily basis. For each recording site, multiple sessions of STN stimulation were made at the frequencies described above and, for each session, continuous recordings were collected 30 s before and 8 to 42 s during DBS. Extracellular action potentials were acquired through platinum-iridium microelectrodes (tip exposure: 10 to 20 μm; impedance: 0.4 to 0.6 MΩ; FHC, Inc., Bowdoinham, ME).

Electrophysiological signals were band pass-filtered and digitally converted (sampling rate: 25 kHz) for off-line analyses. Validated off-line software was used to isolate and remove the stimulus artifacts and to discriminate the action potentials from the background noise [31].

Four months after the beginning of the study, the animal received an initial infusion of MPTP via the right intracarotid artery (0.04mg/kg) followed by three systemic doses of 0.2mg/kg, administered intravenously over the course of several weeks, until the animal demonstrated a consistent motor impairment. Effects of the treatment were assessed by observing the animal’s spontaneous cage behavior. Because stimulation was applied only while the animal was restrained in the chair, no formal clinical assessment of the effects of DBS was conducted.

## B. Point Process Modeling

We formulated point process models (PPMs) to relate the spiking propensity of neurons in the striatum to their own spiking history, the history of other neurons simultaneously recorded (same ensemble), and the DBS pattern. We used the model parameters to analyze the effects of DBS and neuronal synchronization.

A neuronal spike train is treated as a series of random binary events (0s and 1s) that occur continuously in time (point process), where the 1s are spike times and the 0s the times at which no spikes occur [21]–[23]. A PPM of a neural spike train is completely characterized on any interval $(0, T]$ by defining the conditional intensity function (CIF)

$$\lambda(t \mid H_t) = \lim_{\Delta \to 0} \Pr(N(t+\Delta) - N(t) = 1 \mid H_t)/\Delta \tag{1}$$

where $N(t)$ is the number of spikes counted in the interval $(0, t]$ for $t$ in $(0, T]$, $H_t$ is the history of spikes up to time $t$ and Pr $(\cdot)$ is the probability [21]. $\lambda(t|H_t)$ is a generalized history-dependent rate function and $\lambda(t|H_t)\Delta$ approximately gives the spiking propensity at time $t$ if $\Delta$ is small [21]. Because the CIF completely characterizes a spike train, defining a model for the CIF defines a model for the spike train [23]. For each neuron, we defined the following model structure:

$$\lambda(t \mid H_t, \Theta) = e^{\sigma} \lambda_O\left(t \mid H_t^O, \Theta\right) \cdot \lambda_E\left(t \mid H_t^E, \Theta\right) \cdot \lambda_S\left(t \mid H_t^S, \Theta\right) \tag{2}$$

where $e^{\sigma}$ (in spikes/s) accounts for the average history-independent (i.e., Poisson-like) activity, and $\lambda_O$, $\lambda_E$, and $\lambda_S$ are dimensionless functions of the neuron's own spiking activity $H_t^O$, the spiking activity $H_t^E$ of any other neuron in the same ensemble, and the DBS stimulus sequence $H_t^S$ (if applied), respectively. $\Theta$ is a parameter vector to be estimated from data. We set $\Delta$ = 1 ms and assumed that $\lambda_O$, $\lambda_E$, and $\lambda_S$ belong to the class of generalized linear models [32]:

$$\log(\lambda_O) = \sum_{r=1}^{10} \beta_r dN(t - r\Delta, t - (r+1)\Delta) + \sum_{r=11}^{18} \beta_r dN(t - 5(r-8)\Delta, t - 5(r-9)\Delta) \tag{3}$$

$$\log(\lambda_E) = \sum_{q=1}^{Q} \left\{ \sum_{h=1}^{10} \delta_{h,q} dN_q(t - h\Delta, t - (h-1)\Delta) + \sum_{r=11}^{18} \delta_{h,q} dN_q(t - 5(h-8)\Delta, t - 5(h-9)\Delta) \right\} \tag{4}$$

$$\log(\lambda_S) = \sum_{v=1}^{8} \gamma_v dN_S(t - v\Delta, t - (v-1)\Delta) \tag{5}$$

where $dN(a, b)$ and $dN_q(a, b)$ are the number of spikes fired by the given neuron or the $q$-th neuron in the ensemble in the interval $(a, b)$ (in ms), $dN_q(a, b)$ is the number of DBS pulses, and $\Theta = \left[\sigma, \beta_1, \ldots, \beta_{18}, \gamma_1, \ldots, \gamma_8, \left\{\delta_{1,q}, \ldots, \delta_{18,q}\right\}_{q=1}^{Q}\right]$.

For each neuron, with and without DBS, an estimation of the parameter vector $\Theta$ and 95% upper and lower confidence bounds was provided by maximizing the likelihood of observing the recorded spike trains [23][25]–[29]. For each neuron, 80% of spike trains were for parameter estimation and the last 20% for validation.

The set of history bins (i.e. $a$, $b$ in $dN(a, b)$) in (2–5) was chosen by minimizing the Akaike's criterion [33]. The goodness-of-fit of each PPM was assessed on the validation data set with

the Kolmogorov-Smirnov (KS) plot after time rescaling of the spike trains [23]. Only neurons whose PPM passed this test were included in this study. See Table I for the number of neurons considered for each setting.

### C. Statistical Inferences from Point Process Models

Since the spiking propensity $\lambda$ in (2) is given by a Poisson factor ($e^{\sigma}$) modulated by history-dependent factors (i.e., $\lambda_0$, $\lambda_E$, and $\lambda_S$), the neuron's own spiking pattern, the dependency from other neurons, and the response to DBS stimuli depend on the dynamics of $\lambda_0$, $\lambda_E$, $\lambda_S$, respectively. Such dynamics can be non-stationary and is captured by parameters $\Theta$ in (3–5), as $\Theta$ were estimated from the neuron's own spike trains [24][27]. Therefore, we inferred recurrent patterns (RPs) and ensemble inter-neuronal dependencies (INDs) by looking at the 95% confidence bounds of $\{\beta_r\}$ and $\{\delta_{h,q}\}$ in $\Theta$.

We say that a neuron has an RP with period $\Delta_p$ if, at any time $t$, the probability that it spikes is higher than the probability for $e^{\sigma}$, provided that the neuron spiked $\Delta_p$ ms earlier. We inferred an RP with period in $(a, b)$ if the lower 95% confidence bound of $e^{\beta_r}$ (i.e., $\ell_{\beta_r}$) in $\lambda_0$ was $\ell_{\beta_T} > 1.05$, where $\beta_r$ multiplies the number of spikes $dN(a, b)$ in (3), i.e., we inferred an RP if the probability of spiking at a generic $t$ increased by more than 5% over $e^{\sigma}$, given that a spike occurred $(a, b)$ ms before $t$.

Given a pair of neurons $(n_1,n_2)$ in the same ensemble (i.e., simultaneously recorded), we say that $n_1$ has an IND with lag $L_p$ on $n_2$ if, at any time $t$, the probability that $n_1$ spikes is higher than the probability for $e^{\sigma}$, provided that $n_2$ spiked $L_p$ ms earlier. We inferred an IND between the modeled neuron and any other neuron $q$ simultaneously recorded in the same ensemble with lag in $(a, b)$ if the lower 95% confidence bound of $e^{\delta_{h,q}}$ (i.e., $\ell_{\delta_{h,q}}$) in $\lambda_E$ was $\ell_{\delta_{h,q}} > 1.05$, where $\delta_{h,q}$ multiplies the number of spikes $dN_q(a, b)$ in (4).

## III. RESULTS

A total of 166 striatal neurons were recorded (Table I). 25 of them (4 normal, 21 MPTP) were located in the dorsomedial side of striatum (caudate nucleus) and the remaining 141 (95 normal, 46 MPTP) were located in the dorso-lateral side of striatum (putamen).

### A. Poisson Factor in Normal Conditions

For each neuron, it was preliminary tested whether the discharge rate changed significantly (either increased or decreased) during DBS versus rest conditions and it was found that (i) the percentage of neurons with significant change was small under low frequency (LF, <100 Hz) DBS (17.1±13.2%, mean±std.dev.) and (ii) no trend was noticeable as the frequency increased (Fig. 2b). 130 Hz DBS, instead, affected a higher percentage of neurons (56.3%, Fig. 2b), with a significant increment over the fraction of responsive cells measured under LF DBS (t-test, $p<0.0007$). The population-mean discharge rate, instead, was significantly lower during 130 Hz DBS than at rest (Fig. 2a), thus indicating a decreased discharge activity.

The reduction of the population-mean rate was associated with a reduction of the Poisson factor $e^{\sigma}$ in (2) (Fig. 2c). The Poisson factor accounts for the incidence of covariates and the variability of the discharge patterns across the population. High values of $e^{\sigma}$, indeed, correspond to high variability and low impact of the spiking histories. Furthermore, for any generic neuron $n^*$, if the value of the factor $e^{\sigma}$ is close to the correspondent discharge rate, then the spiking activity of $n^*$ can be approximated on average with a Poisson process with (constant) mean value $\hat{\lambda} \triangleq e^{\sigma}$ i.e., $e^{\sigma}$ measures the similarity between the neuron's own discharge pattern and a Poisson process.

Overall, we found that the Poisson factor decreased when DBS frequencies ≥50Hz were used but the reduction was significant ($p<0.001$) only under high frequency (HF, i.e., 100–130Hz) DBS (Fig. 2c), which suggests an increased pattern regularization during HF DBS. Also, $e^{\sigma}$ was close to the average discharge rate during 30, 50, and 80 Hz DBS, while it was significantly lower than the correspondent average rate during HF DBS, which indicates that HF DBS disrupted pre-existent Poisson-like patterns.

## B. Effects of DBS on Discharge Patterns in Normal Conditions

Point process model parameters in (3)–(4) were used to infer non-stationary recursive patterns (RPs) and inter-neuronal dependencies (INDs). We found that RPs and INDs with periods ranging from 3 to 50 ms occurred in ~20% of neurons at rest (Fig. 3). LF DBS did not significantly vary the occurrence of RPs and INDs, while 130 Hz DBS mainly reduced the recurrent patterns with period ranging from 3 to 7 ms. INDs, instead, were less frequent than RPs and less sensitive to the DBS input under normal condition.

STN DBS evoked a transient post-stimulus modulation of the discharge patterns during the inter-pulse interval, as indicated by the post-stimulus time histogram (PSTH, Fig. 4a,b). The PSTH consists of counts of neuronal discharges in consecutive 0.08ms-long time bins within the inter-stimulus interval following each DBS pulse, normalized to the pre-stimulation baseline activity (z-score) [12]. Values of the z-score >1.96 (<−1.96) indicate significant ($p<0.05$) neuronal activation (inhibition) within the inter-pulse interval and can be used to determine the most likely latency between DBS pulses and neuronal spikes [12].

We found that the percentage of neurons that had a significant activation within an inter-pulse interval increased with the DBS frequency. In particular, we counted the neurons with a significant response in three consecutive windows after the DBS pulse (1.2–2.2, 2.3–4.2, 4.5–6.0ms) and found that such fraction was significantly higher with HF DBS than LF DBS, while the latency between the DBS pulse and the first bin with z-score >1.96 was lower under 130 Hz DBS than other settings (Fig. 2d). Therefore, under HF DBS, distinct neurons in striatum were likely to respond similarly right after a stimulus pulse, with no regards to the pre-stimulation baseline pattern. These facts could be consistent with a larger entrainment of the neurons to the same pattern.

Changes in the PSTH are explained by the point process model parameters $\gamma_v$, $v = 1, \ldots, 8$ in (5). Fig. 4c reports the population-mean value of $e^{\gamma_v}$, $v = 1, \ldots, 8$ both for LF and HF DBS. Analogously to the criteria for RP and IND detection (see section II.C), values $e^{\gamma_v} > 1$ for

any generic neuron $n^*$ indicate that the probability of spiking of at a given time $t$ increases over a baseline Poisson process of similar rate, provided that a DBS pulse was delivered in the past 8 ms before $t$. Fig. 4c indicates that, while the impact of LF DBS on the spiking propensity was generally low and vanishing toward the end of the inter-pulse period (i.e., $e^{\gamma_v} \cong 1$ for all $v$, red and dashed-black lines), HF DBS strongly increased the spiking likelihood, with a peak contribution between 1 and 5 ms (i.e., $2 \leq v \leq 6$, green and blue lines). Also, the average value of parameters $e^{\gamma_v}$ under HF DBS was significantly larger than the value of parameters $e^{\beta_r}$ and $e^{\delta_{h,q}}$ in (3)–(4) (Fig. 5), which means that HF DBS likely elicited a strong phase-locked response in the striatal neurons that presumably overrode the dependency from the previous spiking history.

### C. Effects of DBS in MPTP vs. Normal Conditions

At rest, MPTP decreased the population-mean discharge rate and the Poisson factor (Fig. 2a,c), and increased the fraction of neurons with RPs and INDs ($\chi^2$-test, $p<0.05$) (Fig. 3), which is consistent with emerging (non-stationary) oscillatory patterns. Also, the mean value of parameters $e^{\delta_{h,q}}$ in (4) significantly increased after MPTP for every $h = 1, \ldots, 18$ (t-test, $p<0.05$, Fig. 5b), thus indicating an increased coupling between neurons within the same ensemble under dopamine depletion.

The application of DBS determined two major differences between normal and MPTP conditions. First, while discharge rates and PSTH were similar before vs. after MPTP treatment for LF DBS, 130 Hz DBS significantly reduced the latency between DBS pulse and first post-stimulus response (Fig. 2d). Secondly, while 130Hz DBS had similar effects on RPs and INDs both in the normal and MPTP animal (results after MPTP treatment were less pronounced though), LF DBS had stronger effects after the MPTP treatment and significantly increased the incidence of RPs and INDs (Fig. 3b,c) over the baseline values at rest. Also, a comparison between the population-mean value of parameters $e^{\beta_r}$ and $e^{\delta_{h,q}}$ in (3)–(4) for 30 and 130 Hz DBS shows that 130 Hz DBS determined model parameters close to the rest conditions (Fig. 5a,b), while 30 Hz DBS decreased the impact of discharge patterns longer than 15 ms and increased the effects of more recent discharge histories (i.e., parameters on the left side of the dashed vertical lines in Fig. 5 are close to 1).

Overall, non-stationary patterns and inter-neuronal ensemble dependencies increased under MPTP conditions and were further facilitated by LF DBS. 130 Hz DBS, instead, reduced such features by increasing the probability of short-latency post-stimulus responses and decreasing any late post-stimulus modulation.

## IV. CONCLUSION

A computational framework exploiting point process models and single unit recordings collected in a monkey at rest was used to describe the effects of STN DBS and PD conditions on the neuronal dynamics in the motor striatum.

We found that the striatal neurons show baseline Poisson-like discharge activity with recurrent short-term patterns. Minor changes were reported under low frequency STN DBS

while high frequency STN DBS had a marked impact on a large portion of neurons and caused lower discharge rates and more regular patterns. In particular, under high frequency DBS, several distinct neurons had an increased probability of firing a spike concurrently with the delivery of the DBS pulses, and this could reflect large changes in the ongoing pattern of the sub-threshold excitability. Since the sub-threshold excitability is regulated by polysynaptic thalamo- and cortico-striatal projections, which are ultimately affected by the distal effects of STN DBS on thalamus and cortex (Fig. 1), our results suggest that the effects of high frequency STN DBS on striatum presumably stem from an overlap (reinforcement) between local (feed-forward) subthalamo-fugal input and distal (feedback) input propagated along the basal ganglia-thalamo-cortical loop, as speculated in [5][34]–[36].

In the MPTP-treated animal, instead, we noted decreased baseline activity and enhanced oscillations and ensemble dependencies, which are due to the propagation of recurrent non-stationary pathologic rhythms along the motor loop. Low frequency DBS enhanced these features, while high frequency DBS reduced them both in normal and MPTP state. Our results suggest that the effects of high frequency DBS are insensitive to the pre-existent patterns and, therefore, that a possible therapeutic merit of high frequency DBS is the replacement of pre-existent patterns with more regular ones (masking).

## ACKNOWLEDGMENT

S. V. Sarma was supported by the Burroughs Wellcome Fund CASI Award 1007274, NIH R01NS073118-02, and NSF CAREER Award 1055560. J. T. Gale was supported by the American Parkinson's Disease Association. E. B. Montgomery, Jr. was supported by the Dr. Sigmund Rosen Fund of the University of Alabama at Birmingham.

## REFERENCES

[1]. Koller W, et al. "High-frequency unilateral thalamic stimulation in the treatment of essential and Parkinsonian tremor," Ann. Neurol, vol. 42, 1997, pp. 292–299. [PubMed: 9307249]

[2]. Vitek JL, Hashimoto T, Peoples J, DeLong MR, and Bakay AE, "Acute stimulation in the external segment of the globus pallidus improves Parkinsonian motor signs," Mov. Disord, vol. 19, 2004, pp. 907–915. [PubMed: 15300655]

[3]. Moro E, et al. "Long-term results of a multicenter study on subthalamic and pallidal stimulation in Parkinson's disease," Mov. Disord, vol. 25, 2010, pp. 578–586. [PubMed: 20213817]

[4]. Perlmutter JS, and Mink JW, "Deep brain stimulation," Annu. Rev. Neurosci, vol. 29, 2006, pp. 229–257. [PubMed: 16776585]

[5]. Montgomery EB Jr., and Gale JT, "Mechanisms of action of deep brain stimulation (DBS)," Neurosci. Biobehav. Rev, vol. 32, 2008, pp. 388–407. [PubMed: 17706780]

[6]. Benazzouz A, et al., "Effect of high-frequency stimulation of the subthalamic nucleus on the neuronal activities of the substantia nigra pars reticulata and ventrolateral nucleus of the thalamus in the rat," Neuroscience, vol. 2, 2000, pp. 289–295.

[7]. Dostrovsky JO, et al., "Microstimulation-induced inhibition of neuronal firing in human globus pallidus," J. Neurophysiol, vol. 84, 2000, pp. 570–574. [PubMed: 10899228]

[8]. Baker KB, Montgomery EB Jr., Rezai AR, Burgess R, and Lüders HO, "Subthalamic nucleus deep brain stimulus evoked potentials: physiological and therapeutic implications," Mov. Disord, vol. 17, 2002, pp. 969–983. [PubMed: 12360546]

[9]. Anderson ME, Postupna N, and Ruffo M, "Effects of high-frequency stimulation in the internal globus pallidus on the activity of thalamic neurons in the awake monkey," J. Neurophysiol, vol. 89, 2003, pp. 1150–1160. [PubMed: 12574488]

[10]. Hashimoto T, Elder CM, Okun MS, Patrick SK, and Vitek JL, “Stimulation of the subthalamic nucleus changes the firing pattern of pallidal neurons,” J. Neurosci, vol. 23, 2003, pp. 1916–1923. [PubMed: 12629196]

[11]. Filali MH, Hutchinson WD, Palter VN, Lozano AM, and Dostrovsky JO, “Stimulation-induced inhibition of neuronal firing in human subthalamic nucleus,” Exp. Brain. Res, vol. 156, 2004, pp. 274–281. [PubMed: 14745464]

[12]. Montgomery EB Jr., “Effects of GPi stimulation on human thalamic neuronal activity,” Clin. Neurophysiol, vol. 117, 2006, pp. 2691–2702. [PubMed: 17029953]

[13]. Li S, Arbuthnott GW, Jutras MJ, Goldberg JA, and Jaeger D, “Resonant antidromic cortical circuit activation as a consequence of high-frequency subthalamic deep-brain stimulation,” J Neurophysiol, vol. 98, 2007, pp. 3525–3537. [PubMed: 17928554]

[14]. Hahn PJ, et al. “Pallidal burst activity during therapeutic deep brain stimulation,” Exp. Neurol, vol. 211, 2008, pp. 243–251. [PubMed: 18355810]

[15]. Gale JT, Shields DC, Jain FA, Amirnovin R, and Eskandar EN, “Subthalamic nucleus discharge patterns during movement in the normal monkey and Parkinsonian patient,” Brain Res, vol. 1260, 2009, pp. 15–23. [PubMed: 19167367]

[16]. Johnson MD, Vitek JL, and McIntyre CC, “Pallidal stimulation that improves Parkinsonian motor symptoms also modulates neuronal firing patterns in primary motor cortex in the MPTP-treated monkey,” Exp. Neurol, vol. 219, 2009, pp. 359–362. [PubMed: 19409895]

[17]. Montgomery EB Jr., Huang H, Walker HC, Guthrie BL, and Watts RL, “High-frequency deep brain stimulation of the putamen improves bradykinesia in Parkinson’s disease,” Mov. Disord, vol. 26, 2011, pp. 2232–2238. [PubMed: 21714010]

[18]. Kreitzer AC, “Physiology and pharmacology of striatal neurons,” Annu. Rev. Neurosci, vol. 32, 2009, pp. 127–147. [PubMed: 19400717]

[19]. Gale JT, “Basis of periodic activities in the BG-thalamic-cortical system of the rhesus macaque,” Ph.D. dissertation, Kent State Univ., Ohio, 2004.

[20]. Montgomery EB Jr., and Buchholtz SR, “The striatum and motor cortex in motor initiation and execution,” Brain Res, vol. 549, 1991, pp. 222–229. [PubMed: 1884216]

[21]. Snyder DL, and Miller MI, Random Point Processes in Time and Space. New York, NY: Springer, 1991.

[22]. Frank LM, Eden UT, Solo V, Wilson MA, and Brown EN, “Contrasting patterns of receptive field plasticity in the hippocampus and the entorhinal cortex: an adaptive filtering approach,” J. Neurosci, vol. 22, 2002, pp. 3817–3830. [PubMed: 11978857]

[23]. Brown EN, Barbieri R, Eden UT, and Frank LM, “Likelihood methods for neural data analysis,” in Computational Neuroscience: A Comprehensive Approach, Feng J, Ed. London, UK: CRC, 2003, pp. 253–286.

[24]. Truccolo W, Eden UT, Fellows MR, Donoghue JP, and Brown EN, “A point process framework for relating neural spiking activity to spiking history, neural ensemble, and extrinsic covariate effects,” J. Neurophysiol, vol. 93, 2005, pp. 1074–1089. [PubMed: 15356183]

[25]. Pillow JW, et al. “Spatio-temporal correlations and visual signaling in a complete neuronal population,” Nature, vol. 454, 2008, pp. 995–999. [PubMed: 18650810]

[26]. Truccolo W, Hochberg LR, and Donoghue JP, “Collective dynamics in human and monkey sensorimotor cortex: predicting single neuron spikes,” Nat. Neurosci, vol. 13, 2010, pp. 105–111. [PubMed: 19966837]

[27]. Sarma SV, et al. “Using point process models to compare neural spiking activity in the subthalamic nucleus of Parkinson’s patients and a normal primate,” IEEE Trans. Biomed. Eng, vol. 57, 2010, pp. 1297–1305. [PubMed: 20172804]

[28]. Santaniello S, Gale JT, Montgomery EB Jr., and Sarma SV, “Modeling the effects of Deep Brain Stimulation on sensorimotor cortex in normal and MPTP conditions,” in Proc. 32nd IEEE Eng Med Biol Soc, Buenos Aires, AR, 2010, pp. 2081–2084.

[29]. Saxena S, Santaniello S, Montgomery EB Jr., Gale JT, and Sarma SV, “Point process models show temporal dependencies of basal ganglia nuclei under deep brain stimulation,” in Proc. 32nd IEEE Eng Med Biol Soc, Buenos Aires, AR, 2010, pp. 4152–4155.

[30]. Santaniello S, Gale JT, Montgomery EB Jr., and Sarma SV, “Reinforcement mechanisms in putamen during high frequency STN DBS: A point process study,” in Proc. 34th IEEE Eng Med Biol Soc., San Diego, CA, 2012, pp. 1214–1217.

[31]. Montgomery EB Jr., Gale JT, and Huang H, “Methods for isolating extracellular action potentials and removing stimulus artifacts from microelectrode recordings of neurons requiring minimal operator intervention,” J. Neurosci. Methods, vol. 144, 2005, pp. 107–125. [PubMed: 15848245]

[32]. McCullagh P, and Nelder JA, Generalized Linear Models, 2nd ed., Boca Raton, FL: CRC, 1990.

[33]. Akaike H, “A new look at the statistical model identification,” IEEE Trans. Aut. Control, vol. 19, 1974, pp. 716–723.

[34]. Montgomery EB Jr., and Baker KB, “Mechanisms of deep brain stimulation and future technical developments,” Neurol. Res, vol. 22, 2000, pp. 259–266. [PubMed: 10769818]

[35]. Montgomery EB, “Dynamically coupled, high-frequency reentrant, nonlinear oscillators embedded in scale-free basal ganglia-thalamiccortical networks mediating function and deep brain stimulation effects,” Nonlinear Studies, vol. 11, 2004, pp. 385–421.

[36]. Montgomery EB, “Basal ganglia physiology and pathophysiology: a reappraisal,” Parkinsonism Relat. Disord, vol. 13, 2007, pp. 455–465. [PubMed: 17977052]

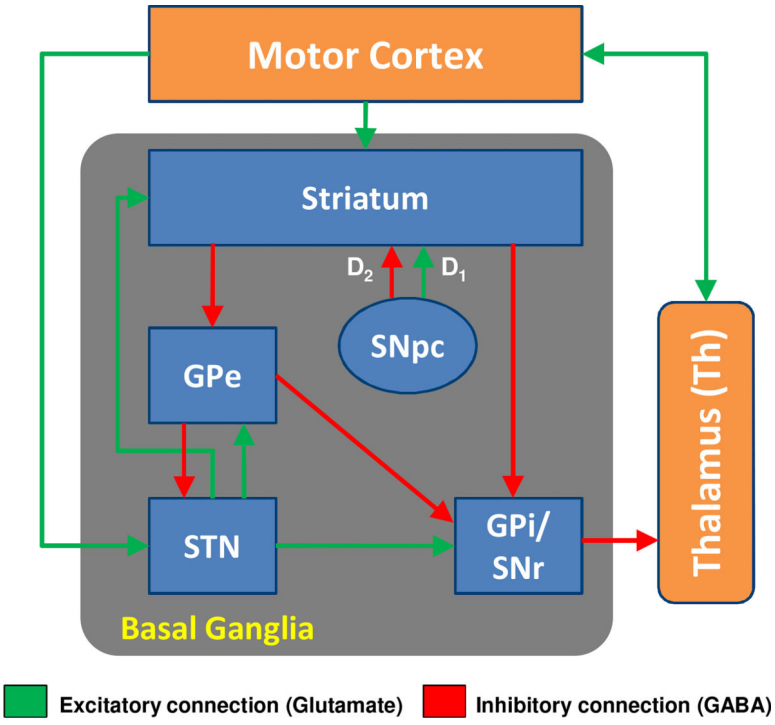


**Fig. 1.**

Motor loop schematic. Basal Ganglia (gray box) include the following nuclei: striatum, globus pallidus (GPe and GPi), substantial nigra (SNpc and SNr), and subthalamic nucleus (STN). $D_1$, $D_2$ = dopaminergic transmitters.

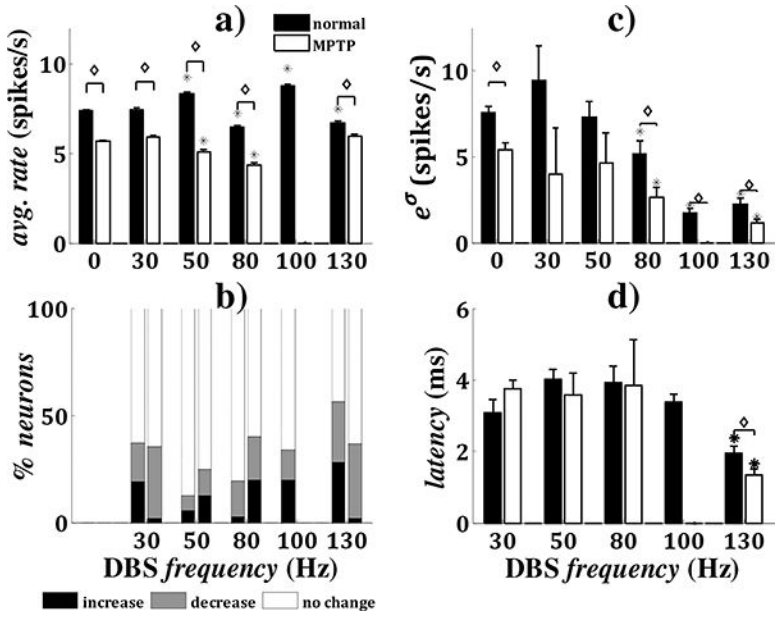


**Fig. 2.**

a) Population-mean discharge rate at rest (0 Hz) and during STN DBS. b) Percentage of neurons that increase, decrease or not significantly change the discharge rate during DBS vs. rest. c) Population-mean value of the Poisson factor $e^{\sigma}$ in (2). d) Population-mean latency between the DBS pulses and the first post-stimulus spike in activated neurons. In a), c), and d): values are mean ± s.e.m.; asterisks denote significant differences during DBS vs. rest; for each DBS setting, diamonds denote significant differences in MPTP vs. normal conditions. Significance: t-test, $p<0.001$ (a,c); 1-way ANOVA with Tukey's post-hoc test, $p<0.05$ (d).

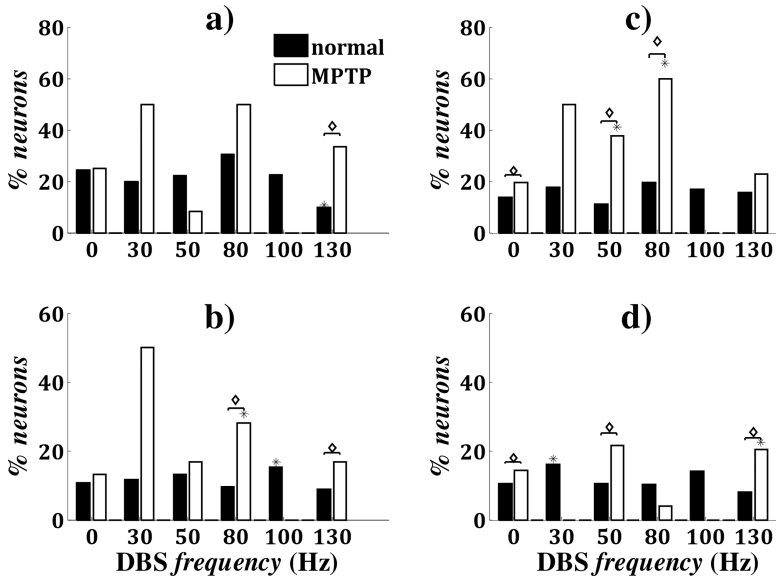


**Fig. 3.**

a,c) Percentage of neurons with RPs of period in the range 3–7 ms (a) and 30–50 ms (c), respectively. b,d) Percentage of neurons with INDs of lag in the range 10–30ms (b) and 30–50 ms (d), respectively. Asterisks denote significant differences during DBS vs. rest. For each DBS setting, diamonds indicate significant differences between MPTP and normal conditions. Significance: $\chi^2$-test, $p<0.05$.

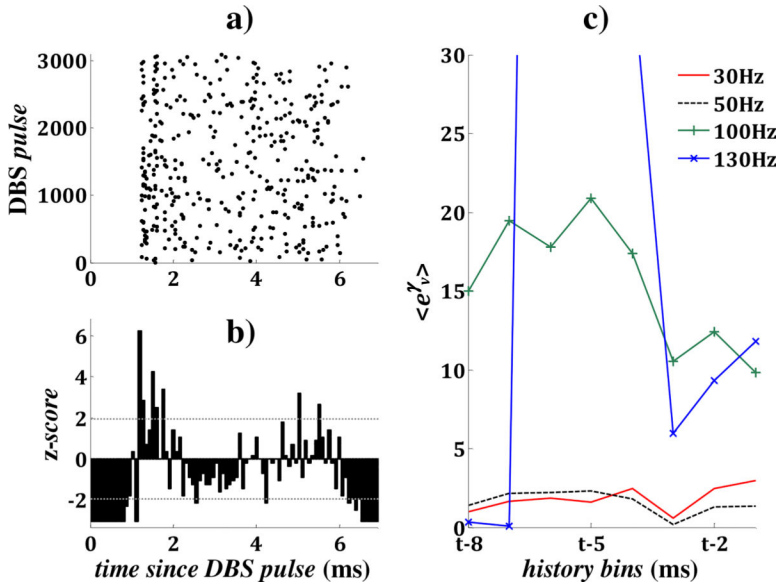


**Fig. 4.**

a,b) Post-stimulus time raster of a neuron (a) during 130 Hz DBS (normal conditions) and correspondent post-stimulus time histogram (PSTH) normalized to the pre-DBS activity (b). Dotted lines indicate significance levels (±1.96). c) Population-mean value of the model parameters $e^{\gamma_v}$, $v = 1,\ldots,8$ for several DBS frequencies in normal conditions. Parameters were depicted vs. the history bins for a generic time $t$. Parameters estimated during 130 Hz STN DBS reach a peak value of 157 for $v = 5$ (blue line, data truncated at top).

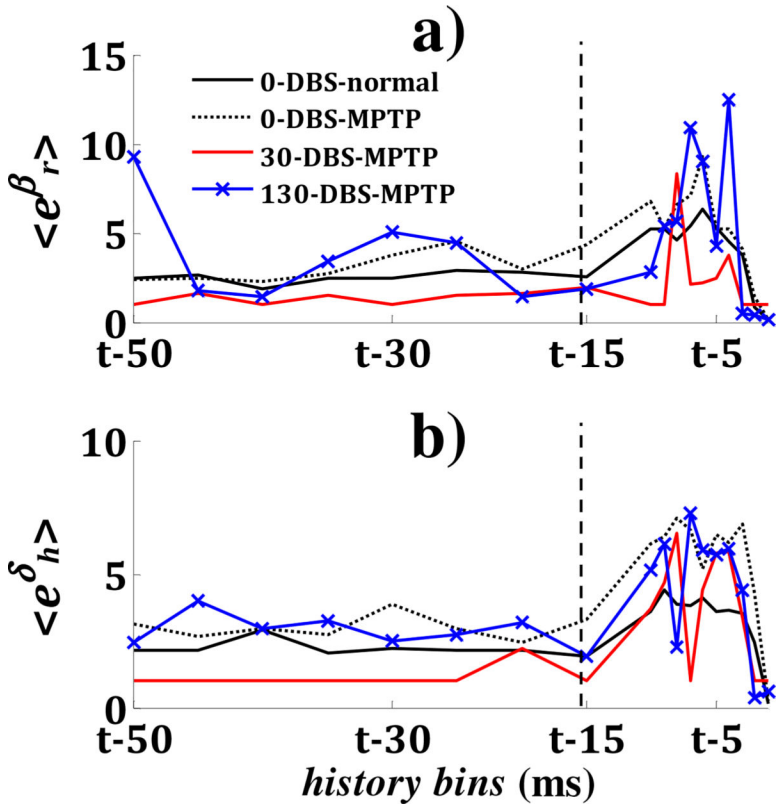


**Fig. 5.**

Population-mean value of the point process model parameters $e^{\beta_r}$, $r = 1, \ldots, 18$ (a) and $e^{\delta_h}$, $h = 1, \ldots, 18$ (b). Parameters were depicted vs. the history bins for a generic time $t$. In the legend: 0-DBS-normal = parameters estimated at rest (no DBS) under normal conditions. ##-DBS-MPTP = parameters estimated under DBS at frequency ## Hz in the MPTP-treated animal, with ## = 0, 30, or 130.

**TABLE I**

Experimental Dataset

| | DBS Frequency (Hz) | Normal | MPTP |
|---|---|---|---|
| # of Neurons | no DBS | 99 | 67 |
| | 30 | 71 | 49 |
| | 50 | 72 | 24 |
| | 80 | 36 | 10 |
| | 100 | 71 | - |
| | 130 | 52 | 49 |
| # of Neuron Pairs | no DBS | 334 | 237 |
| | 30 | 248 | 175 |
| | 50 | 258 | 91 |
| | 80 | 167 | 25 |
| | 100 | 268 | - |
| | 130 | 141 | 175 |